

However, riverine-dissolved inorganic nutrients and terrestrial organic carbon inputs are not significant relative to those provided via the upwelling process, which fuels autotrophic production in the basin. Upwelling leads to an input of upper (~150 m) Caribbean Sea water into the basin containing nutrients and dissolved inorganic carbon, and combined with a deeper mixed layer, nutrient inputs to surface waters fuel annual primary production of approximately  $3 \times 10^{11} \text{ mol C yr}^{-1}$  over the area of the upwelling plume (~7,000 km<sup>2</sup>). At the depth of the oxic–anoxic interface, which itself fluctuates between depths of about 275 and 350 m, an 80–100 m thick chemoautotrophic layer occurs. Like photoautotrophic production in the surface layer, chemoautotrophic production within the redox cline has varied about 20-fold over our observation period, with the average rate of chemoautotrophic bacterial production over our period of study being equivalent to about 70% of surface production. This material does not seem to sink and therefore seems to be recycled within this layer.

Losses of carbon dioxide to the atmosphere are approximately of the same magnitude as losses of particulate organic carbon to depths greater than 275 m in the basin, or about  $1.6 \times 10^{10} \text{ mol C}$  integrated over the area of the plume. However, these losses combined are about an order of magnitude smaller than possible exports in the form of lateral advection of dissolved inorganic and particulate organic material out of the Cariaco Basin. Such lateral losses over the course of a year are likely significant, since the entire upper water column in the basin is replaced at least once a year.

In order to fully understand this cycle, how it varies over long timescales and how signals of climate variation are recorded at the bottom of the Cariaco Basin in laminated sediments will require maintaining a robust time series of observations. These observations will also be helpful to understand how biogeochemical signals in the North Atlantic are propagated from mid-latitudes to tropical regions and vice versa, when combined with measurements collected at other time series stations in this basin, such as the Bermuda-Atlantic time series station (BATS, Bermuda), the European Station for time-series in the ocean (ESTOC, Canary Islands), and the Tropical Eastern North Atlantic time-series observatory (TENATSO, Cape Verde).

## 8.6 The South China Sea<sup>2</sup>

K.-K. Liu, C.-M. Tseng, C.-R. Wu  
and I.-I. Lin

South China Sea (SCS), which spans from 1.5 to 23°N, is located in tropical Southeast Asia (Fig. 8.6.1). It has extensive continental shelves to the northwest and south in contrast with the deep basin in the central region (Fig. 8.6.1). The surrounding landmasses and islands make the SCS a semi-enclosed water body, which may be viewed as the Mediterranean Sea of the western Pacific Ocean. Unlike the Mediterranean Sea the rainfall is high in this region because of monsoons and typhoons. The many channels and passages between the SCS and its surroundings make water exchange considerably faster than that of the Mediterranean Sea.

The biogeochemistry of the SCS is dynamic and potentially sensitive to climate change. Such a premise has inspired new observations and modeling work that were undertaken in recent years for the exploration of the SCS (e.g., Liu et al. 2002; Wong et al. 2007). A major source of information for this synthesis is the South-East Asia Time-series Study (SEATS). Its main purpose is to understand how physical forcing at various timescales controls biogeochemical cycles in the South China Sea. Bimonthly or quarterly cruises have been conducted to survey the SEATS station (18.0°N, 115.6°E, S1 in Fig. 8.6.1) since September 1999 (Tseng et al. 2005). A better understanding of SCS biogeochemistry is essential for the interpretation of paleo records in the SCS, which have been systematically studied recently (e.g., Huang et al. 1997; Wang et al. 1999), and may facilitate the prediction of future changes in this regional marine ecosystem.

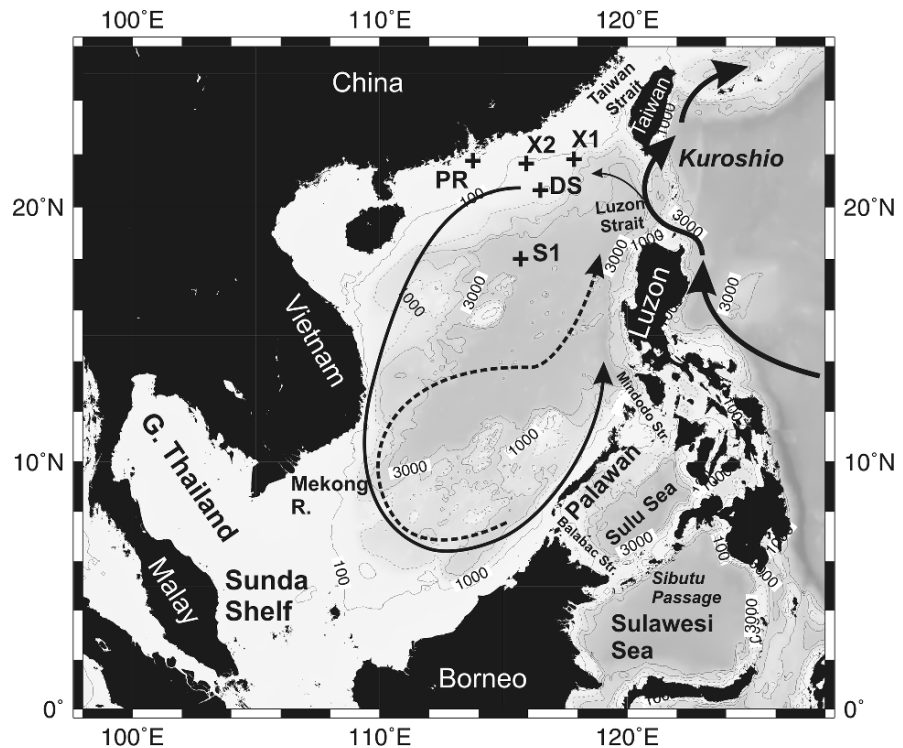
---

K.-K. Liu (✉)

Institute of Hydrological & Oceanic Sciences, National Central University, Jungli, Taiwan 32001, ROC  
e-mail: kkliu@ncu.edu.tw

<sup>2</sup> This article benefits from critical reviews of Fred Mackenzie, Neal Blair, and an anonymous reviewer, whose comments improved the quality of this article. This work was supported by grants from the National Science Council (ROC). This is NCU-IHOS contribution no. 92.

**Fig. 8.6.1** SCS bathymetry. For this study the northern and southern border of the SCS domain are 24 and 1.5°N, respectively; the eastern border is along the sill of the Luzon Strait between Luzon and Taiwan. Circulation in and near the SCS is indicated by the *curved arrows*. The *thin curved arrow* indicates the circulation in winter. The *dashed arrow* indicates the circulation in summer. The *thick arrows* indicate the path of the Kuroshio



## 8.6.1 Environmental Setting

### 8.6.1.1 Geography and Meteorological Conditions

The SCS has a total area of 3.35 million km<sup>2</sup>; 40.5% of it is the shelf, defined as regions with bottom depths less than 100 m, and the remainder is the interior, where the depth attains a maximum of 5,006 m (NGDC 2001). The SCS is surrounded by southwestern China and Taiwan to the north, by Vietnam to the west and the Philippines to the east, and by Malay and Borneo to the southwest and southeast, respectively (Fig. 8.6.1). It is connected to the West Philippine Sea (WPS) through the Luzon Strait between Taiwan and Luzon, which has an effective sill depth around 2,000 m and serves as the only channel for exchange of deep water with the ocean outside. The SCS is connected with the Sulu Sea (Fig. 8.6.1) through the Mindoro Strait between Luzon and Palawan and the shallow Balabac Strait between Palawan and Borneo (Wyrтки 1961). The Mindoro Strait has a sill depth of 420 m. The Sulu Sea is con-

nected to the WPS through shallow passages with sill depths shallower than 110 m; it is also connected to the Sulawesi Sea through the Sibutu Passage, which has a sill depth of 250 m. Therefore, the route through the Mindoro Strait–Sibutu Passage allows some exchange of the intermediate water between the SCS and the WPS, but the volume is limited. The Taiwan Strait to the north and the Sunda Shelf to the south are rather shallow (ca. 60 m) so that only the exchange of surface waters is permitted (Fig. 8.6.1).

The SCS experiences the southwest monsoon from May to August and the northeast monsoon from October to March of the next year. The northeast monsoon is usually stronger than the southwest monsoon, but the precipitation is higher during the southwest monsoon (Fig. 8.6.2). The SCS is frequently invaded by typhoons. From 1950 to 2001 there were on average 10 typhoons invading the SCS every year (<https://metoc.npmoc.navy.mil/jtwc.html>). Most typhoons occurred to the north of 10°N from May to October. Typhoons usually bring a considerable amount of rain to the SCS; this explains why the rain is heavier during the SW monsoon period (Fig. 8.6.2).

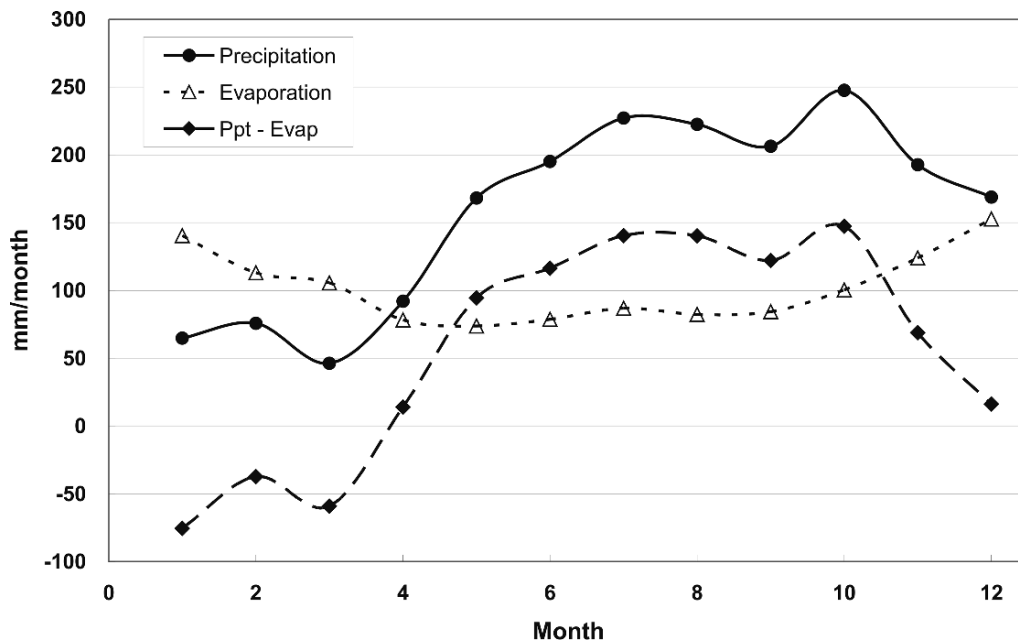


**Fig. 8.6.2** Monthly mean precipitation (Huffman et al. 2001) and evaporation (Chou et al. 2003) in the SCS over an annual cycle for the period January 1997 to December 2000

By contrast, evaporation is stronger under the northeast monsoon. Consequently, from January to March, there is net evaporation; for the rest of the year there is net precipitation (Fig. 8.6.2). The annual mean precipitation is 1,908 mm, while the mean evaporation is 1,220 mm. The net input of water from the atmosphere is about  $688 \text{ mm yr}^{-1}$ , which amounts to a total volume input of  $2,300 \text{ km}^3 \text{ yr}^{-1}$  (Huffman et al. 2001; Chou et al. 2003).

### 8.6.1.2 Circulation and Water Exchange

The currents within the SCS proper are rather weak, whereas the strong western boundary current, namely, the Kuroshio, flows essentially northward by the Luzon Strait with partial intrusion into the SCS (Fig. 8.6.1). In winter the intrusion is most evident with high salinity water entering the SCS proper (Shaw 1991) and following the cyclonic circulation driven by the persistent northeast monsoon (Shaw and Chao 1994). The southward jet off Vietnam partially flows across the Sunda Shelf entering the shallow Java Sea, which has a mean depth of only 43 m and allows only the surface water to enter. The rest of the jet turns cyclonically toward

the east. In summer the southwest monsoon reverses the coastal jet off Vietnam; the northward flow veers off the coast at about  $12^\circ\text{N}$  (Fig. 8.6.1). The seaward current crosses the SCS interior and turns cyclonically in the northern basin (Shaw and Chao 1994).

The exchange of water between the SCS and its surrounding seas has been studied since the 1960s. Wyrki (1961) estimated bimonthly transports through the major exchange channels, namely the Luzon Strait, Taiwan Strait, and Sunda Shelf–Java Sea, which have been used to constrain regional circulation models (e.g., Shaw and Chao 1994; Wu et al. 1999). These estimates give annual mean transports of net inflow of 0.25 Sv from the Luzon Strait, net outflow of the same magnitude through Sunda Shelf–Java Sea, and no net flow through the Taiwan Strait. However, a high-resolution general circulation model predicts the net westward transport through the Luzon Strait to be 2–4 Sv (Qu et al. 2005). Recent measurements in the Taiwan Strait yield estimates of transport through the Taiwan Strait varying between 0.9 and 2.7 Sv in response to the northeast and southwest monsoons (Wang et al. 2003b). The amplitude of observed seasonal variation (1.8 Sv) is similar to that (1.5 Sv) of Wyrki's, but the mean flow is much larger in the northward component. Wu and Hsin (2005) employed nested

Princeton Ocean Models (Blumberg and Mellor 1987) with horizontal resolutions of 1/8–1/16 degree to simulate the flow field in the northwestern North Pacific Ocean, which matches the observations well. Their model output is used as an important source of transport estimates in this synthesis. In his simplified treatment, Wyrki (1961) did not pay attention to the Mindoro Strait. However, Metzger and Hurlburt (1996) pointed out that the cyclonic circulation around Luzon Island (Fig. 8.6.1), mainly through the Luzon and the Mindoro Straits, is an important part of the western boundary current system in the North Pacific Ocean. This is also confirmed by a high-resolution model (Qu et al. 2005).

The water exchange between the WPS and the deep SCS basin is rapid as suggested by similar  $^{14}\text{C}$  abundances in the deep water of the two seas (Broecker et al. 1986a). The deep inflow to the SCS from the WPS has been estimated to be 0.42–1.2 Sv (Wang 1986; Liu and Liu 1988; Gong et al. 1992), implying a mean residence time of 40–150 years. Above the sill depth, the deep upwelling occurs mostly along the northwestern slope and downwelling occurs mostly in the southeastern half. The displaced basin water requires a net deep upwelling. The intermediate water may flow out of the SCS, as suggested by a persistent outward flow through the Luzon Strait at mid-depth around 900 m (Chao et al. 1996a).

Gong et al. (1992) and Chen et al. (2001b) suggested the intermediate layer to be the main outflow of the upwelled SCS basin water. Recently You et al. (2005) analyzed water masses and circulation in the SCS and the North Pacific Ocean and suggested an inflow of 1.1 Sv of intermediate water from the WPS into the SCS. The 3-D model also predicts inflow in the intermediate layer. The lack of strong salinity minimum, which is characteristic of the NPIW, suggests that the inflow of the NPIW is not large and the signal is attenuated by the mixing processes within the SCS basin.

Aside from the large-scale circulation, mesoscale eddies from the North Pacific Ocean may penetrate the Luzon Strait (Yang et al. 2004). The rugged topography over the Luzon Strait and the passages connecting the SCS with the open Pacific Ocean often cause internal solitons that propagate westward as internal waves toward the northwestern shelf of the SCS (Hsu et al. 2000). The breaking internal waves cause strong vertical mixing. We have taken these new findings into con-

sideration when we construct the water and salt budgets to be discussed later.

### 8.6.1.3 Hydrography and Nutrient Distributions

The annual mean distributions of sea surface temperature (SST) and sea surface salinity (SSS) are shown in Fig. 8.6.3 (NODC 1998). The SCS is adjacent to the western Pacific warm pool (WPWP) and therefore has a relatively high SST. The annual mean SST ranges from 25 to 29°C (Chu et al. 1997). The coolest water occurs along the southwestern coast of China and the Vietnamese coast. The former area receives cold coastal water from the area farther north under persistent northeast monsoon conditions (Ko et al. 2003). The latter area experiences upwelling in summer (Chao et al. 1996a).

The salinity is lowest in the Gulf of Tonkin, the Gulf of Thailand, and in the Sunda Shelf adjacent to western Borneo. The Gulf of Tonkin receives runoff from the northern Vietnamese rivers, including the Red River (Table 8.6.1). The Gulf of Thailand has very low salinities with monthly mean surface salinity ranging from 31.7 in February to 32.7 in July and August (Snidovongs 1998). The abundant runoff apparently contributes to the low salinity in the Gulf, but the five major Thai rivers, including the Chao Phraya River (Table 8.6.1), have limited contributions; the nearby Mekong River (Snidovongs 1998) has much higher runoff (Table 8.6.1) so that its outflow intrudes the Gulf during the northeast monsoon in winter resulting in the lowest salinity. The slow water exchange with the open sea also contributes to its low salinity. The low salinity in the Sunda Shelf adjacent to Borneo is attributed to the very high precipitation in western Borneo.

The abundant freshwater from direct precipitation and river runoffs in the SCS makes its surface water distinctively less saline than the adjacent western North Pacific resulting in a salinity front at the Luzon Strait (Fig. 8.6.4). The salinity front exists not only in the surface water but also in the subsurface water (Fig. 8.6.4) as pointed out by Chen and Huang (1996). The cores of the North Pacific Tropical Water indicated by the salinity maximum and the North Pacific Intermediate Water indicated by the salinity minimum all remain east of the Luzon Strait. The TS diagram (Fig. 8.6.5) clearly depicts the contrast in hydrography between the SCS and the western North Pacific.

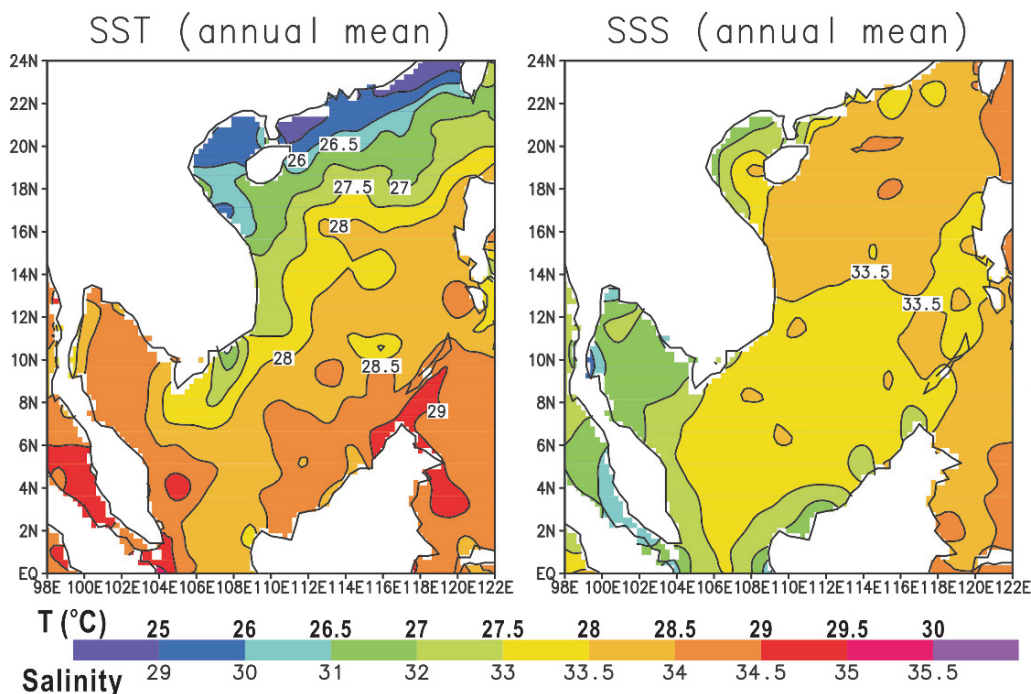


**Fig. 8.6.3** Mean sea surface temperature (SST) and mean sea surface salinity (SSS) in the SCS (NODC 1998)

**Table 8.6.1** River discharges

River	Watershed (1,000 km <sup>2</sup> )	Runoff (km <sup>3</sup> yr <sup>-1</sup> )	Population (million)	DIN (Gmol)	DIP (Gmol)	TSS (Mt yr <sup>-1</sup> )	TDS (Mt yr <sup>-1</sup> )
Zhujiang system	541	300	41	15.4	0.19	80	60
Red River	117	120	20	7.0	0.09	160	70
Mekong	790	470	62	24.1	0.30	160	57
Northwestern Borneo Rivers	150	250	3	6.1	0.08	350	65
Chao Phraya	160	30	45	3.2	0.04	11	5
Other rivers	124	119	35	8.5	0.11	93	31
Sum	1,882	1,289	206	64	0.8	854	288

Although most of the water in the SCS comes from the western North Pacific, its TS characteristics are quite different from those of the latter, which show very strong salinity maxima and minima below the surface layer. By contrast the SCS shows much subdued extreme salinity values in the subsurface water. The very low salinities in the surface water and the coastal zones evidently have influenced waters in the SCS proper. However, the intrusion of the Kuroshio water into the SCS interior in winter (Shaw 1991) is also evident from the TS properties. The hydrocast at the SEATS station in March demonstrated a shift toward higher salinity in the subsurface layer (Fig. 8.6.6) due to the intrusion of the WPS water.

## 8.6.2 External Forcing and Nutrient Fluxes

### 8.6.2.1 Monsoon-Driven Upwelling

The monsoons drive upwelling in three regions in the SCS (Fig. 8.6.1): off northwestern Luzon, around the shelf break in the northern Sunda Shelf in winter, and off the central Vietnamese coast in summer (Chao et al. 1996a; Shaw et al. 1996). It is noted that upwelling is often coupled with downwelling in adjacent regions (Liu et al. 2002). Upwelling and downwelling may occur alternately in certain regions, resulting in effective vertical water exchange or mixing, due to the

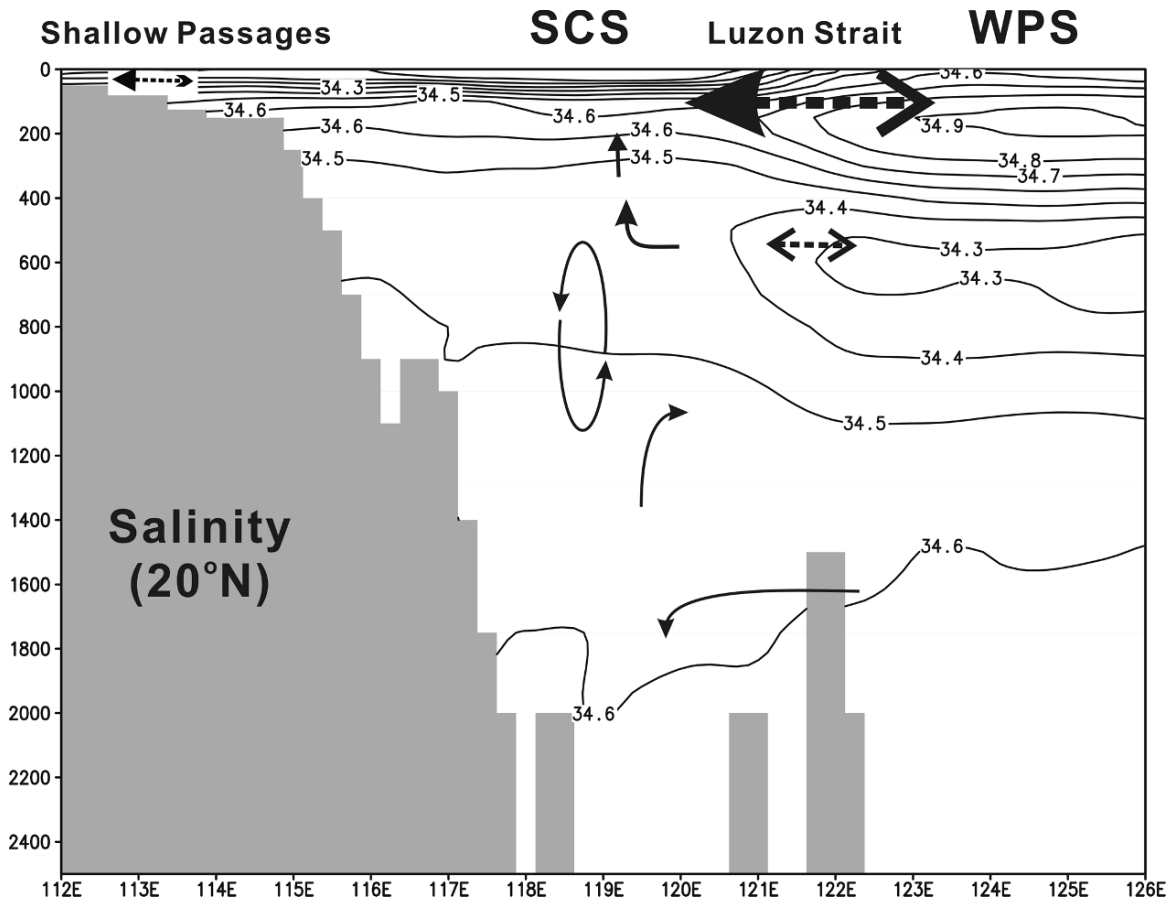


**Fig. 8.6.4** Vertical section of salinity contours along 20°N (NODC 1998). The Luzon Strait is at about 121–122°E, where the salinity front exists between the SCS water and the

West Philippine Sea (WPS) water. The *arrows* indicate water exchange and circulation. The size of the *arrow* is roughly proportional to the transport

alternating monsoons. In the three upwelling regions, the net flow of the vertical exchange is upward transport of the intermediate water.

The upwelling off NW Luzon is attributed to subsurface convergence of the eastern boundary current (Shaw et al. 1996). When the northward flow just west of Luzon converges with the intruding Kuroshio from the Luzon Strait, the subsurface layer tends to thicken and the thermocline moves upward. The positive wind stress curl also induces Ekman suction or upwelling (Chao et al. 1996b). As the southward current in winter impinges on the Sunda Shelf, the subsurface water is uplifted by the shoaling topography, inducing upwelling. The upwelling off Vietnam is induced by the separation of the western boundary current from the Vietnamese coast in summer. The sea-

ward drift causes an upwelling center off Vietnam at about 12°N in summer. The nitrate fluxes associated with upwelling (Fig. 8.6.7) have been estimated by Liu et al. (2002) using a coupled physical–biogeochemical model. Each of the three upwelling regions has an area of about  $2 \times 10^5$  km<sup>2</sup>, which gives a total upwelled nitrate on the order of 1 Gmol d<sup>-1</sup> in each region during the corresponding upwelling season.

### 8.6.2.2 Typhoons and Internal Waves

It has been observed that typhoons drive vertical mixing and upwelling resulting in significant drop of the SST (e.g., Lin et al. 2003). They report elevated Chl-*a* in the cool water patch induced by typhoon Kai-tak in

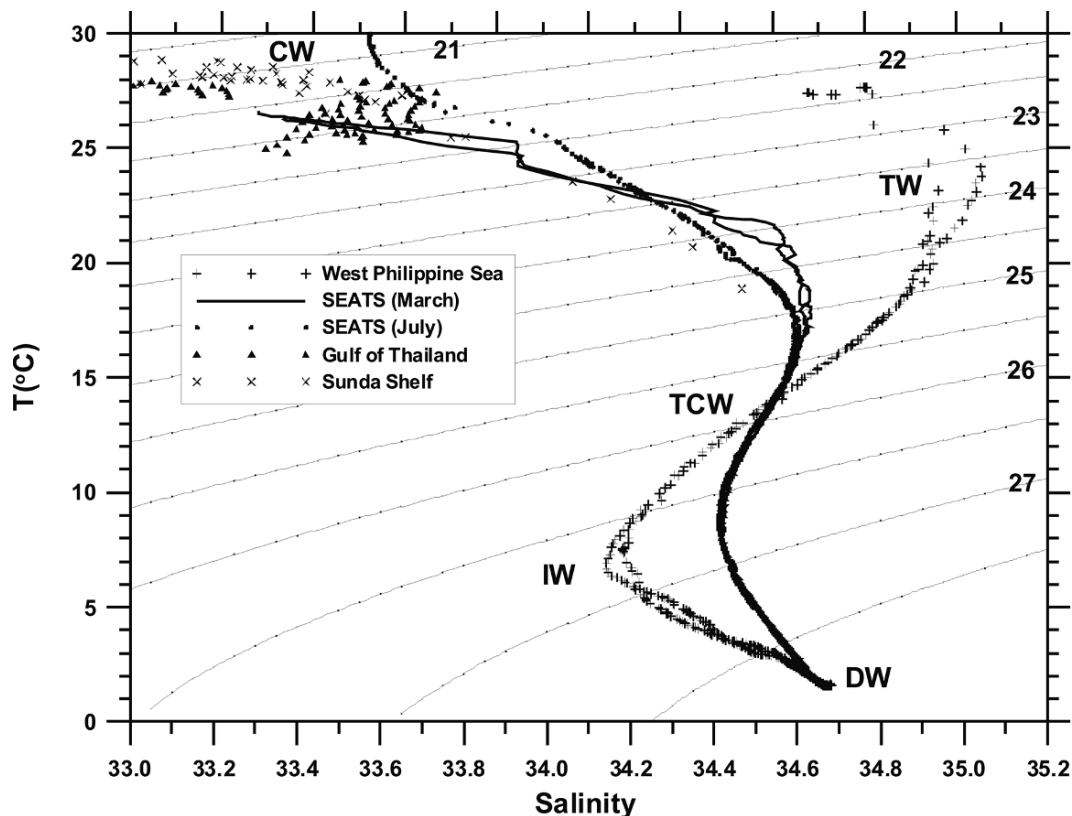


**Fig. 8.6.5** T-S diagram from typical stations in the SCS and the WPS. For the water masses, CM: Coastal Water, TW: Tropical

Water, TCW: Thermocline Water, NPIW: North Pacific Intermediate Water, DW: Deep Water

the northern SCS. The estimated primary production associated with the typhoon-induced patch is 0.8 MtC (67 Gmol C). If 80% of the primary production (PP) is supported by nutrients mixed up from the subsurface layer, the typhoon-driven nutrient pump may transport 8 Gmol N to the surface layer in this event. Because Kai-tak was a moderate typhoon (Category 2), it is likely that half of the typhoons that traverse the SCS may induce similar responses. If this is the case, there are on average about five events per year that may produce a total nutrient transport of 40 Gmol N yr<sup>-1</sup>.

In the northern South China Sea, the surface manifestation of many internal waves has been delineated by synthetic aperture radar images from the ERS-1 and ERS-2 satellites (Hsu et al. 2000). The internal wave breaking may pump up nutrients to the surface layer. Chemical hydrography obtained in the northern SCS (Su 2004) reveals elevated nutrient concentrations in the upper water column in the area, where

internal waves reach the shoaling shelf. Figure 8.6.8 shows the profiles of elevated phosphate concentration in the water column.

### 8.6.2.3 River Discharges and Atmospheric Deposition

The heavy rainfall brings abundant river runoff (1,289 km<sup>3</sup> yr<sup>-1</sup>) to the SCS. The data on river discharges are listed in Table 8.6.1. The Mekong River is the largest river in this region, followed by the Pearl River. Combined they provide 36% of the total runoff to the SCS. The dissolved inorganic nitrogen (DIN) loads are calculated from the mean runoff depth and population density of the watersheds (Smith et al. 2003b). The two largest rivers provide about 50% of the total DIN loading. The loadings of dissolved inorganic phosphorus (DIP) are calculated from the DIN loadings under the assumption of a constant N:P ratio

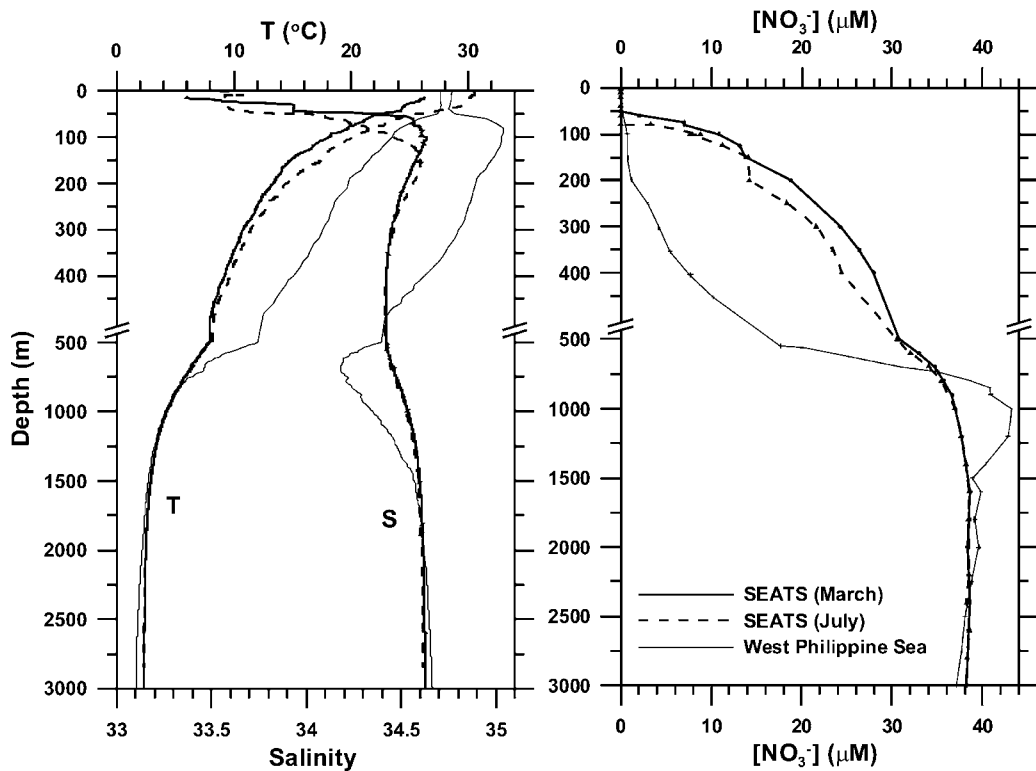


**Fig. 8.6.6** Chemical hydrography in the SCS and the WPS. (a) Profiles of temperature and salinity; (b) Profiles of nitrate. (Data from NCOR and from Gong et al. 1992)

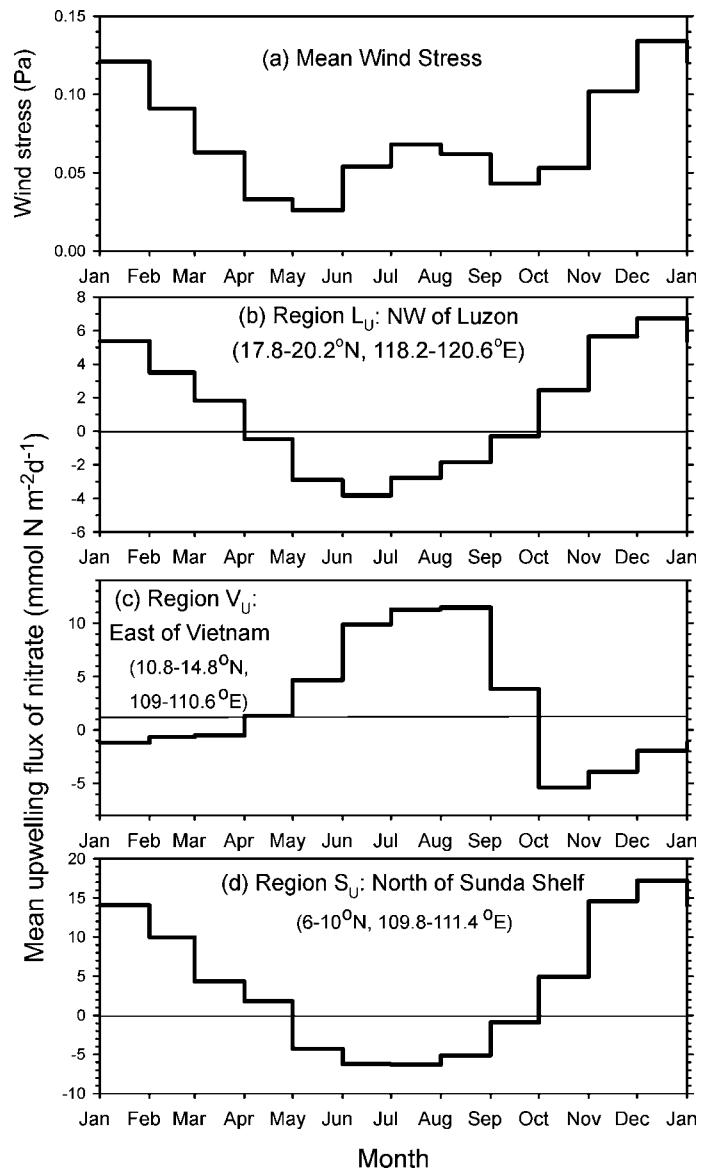
of 80 (Chen et al. 2001b). The unusually low DIP abundance relative to DIN is characteristic of many East Asian rivers, including the Pearl River (Cai et al. 2004). By contrast, the largest exporter of sediments is neither of the two largest rivers but belongs to the smaller rivers of northwestern Borneo (Milliman et al. 1999a), where the relief is steep and the rainfall is extremely high (approaching 3,000 mm yr<sup>-1</sup>).

The total riverine load of dissolved organic carbon is estimated to be 226 Gmol C yr<sup>-1</sup> under the assumption of a mean concentration of 2.1 mg CL<sup>-1</sup> in the runoff, which is the mean DOC concentration reported for Changjiang (Harrison et al. 2005a) and the Lanyang Creek (Kao and Liu 1997). The latter is a typical river in the Southeast Asian region of high rainfall. This flux implies a mean production rate of 1.4 g C m<sup>-2</sup> yr<sup>-1</sup>, which is consistent with model predicted yields in this region (Harrison et al. 2005a). The total riverine load of particulate organic carbon is estimated to be 408 Gmol C yr<sup>-1</sup> under the assumption of a mean yield

of 1.4 g C m<sup>-2</sup> yr<sup>-1</sup> in the drainage area, which is the average of the major river basins in this region (Beusen et al. 2005).

The atmospheric input of macro- and micronutrients to the SCS has not been well studied. For the dry and wet deposition of inorganic nitrogen, the flux in the SCS is probably similar to those (4–10 mmol N m<sup>-2</sup> yr<sup>-1</sup>) in the Bermuda or Barbados regions (Prospero et al. 1996). If we assume a mean flux of 7 mmol N m<sup>-2</sup> yr<sup>-1</sup>, the total input amounts to 23 Gmol N yr<sup>-1</sup>. The atmospheric deposition of inorganic phosphorus is associated with dust deposits, which also carry aeolian iron fluxes. The atmospheric deposition of iron in the SCS is estimated to be around 300 mg m<sup>-2</sup> yr<sup>-1</sup> (Duce and Tinsdale 1991). If the Fe:P ratio of the dust in the SCS is similar to that (30:1) in the north Atlantic Ocean (Prospero et al. 1996) the aeolian phosphorus flux would be 10 mg m<sup>-2</sup> yr<sup>-1</sup> or 0.32 mmol m<sup>-2</sup> yr<sup>-1</sup>, which gives a total amount of 1.1 Gmol P yr<sup>-1</sup>.

**Fig. 8.6.7** (a) Monthly mean wind stress over the SCS. (b–d) Modeled monthly mean vertical DIN fluxes in three upwelling areas (Liu et al. 2002)



### 8.6.3 Biogeochemical Cycles

#### 8.6.3.1 Primary Production, Export Production, and Organic Carbon Burial

The chlorophyll distribution and primary production in the SCS are closely related to monsoon-driven upwelling as demonstrated by a coupled physical–biogeochemical model (Liu et al. 2002). Elevated chlorophyll concentrations occur in the northern SCS off northwest Luzon and over the Sunda Shelf under

the northeast monsoons in winter (Fig. 8.6.9a) and off the Vietnam coast under the southwest monsoon in summer (Fig. 8.6.9b), while the lowest values occur during the inter-monsoon periods. The winter maxima are stronger and more extensive than the summer maxima under the southwest monsoon, which is weaker than the northeast monsoon.

Using a modified biogeochemical scheme, Liu et al. (2007a) reevaluated primary production in the SCS. The model predicts considerable seasonal variation of IPP (integrated primary production) with maxima (up to monthly mean of  $674 \text{ mg C m}^{-2} \text{ d}^{-1}$ )

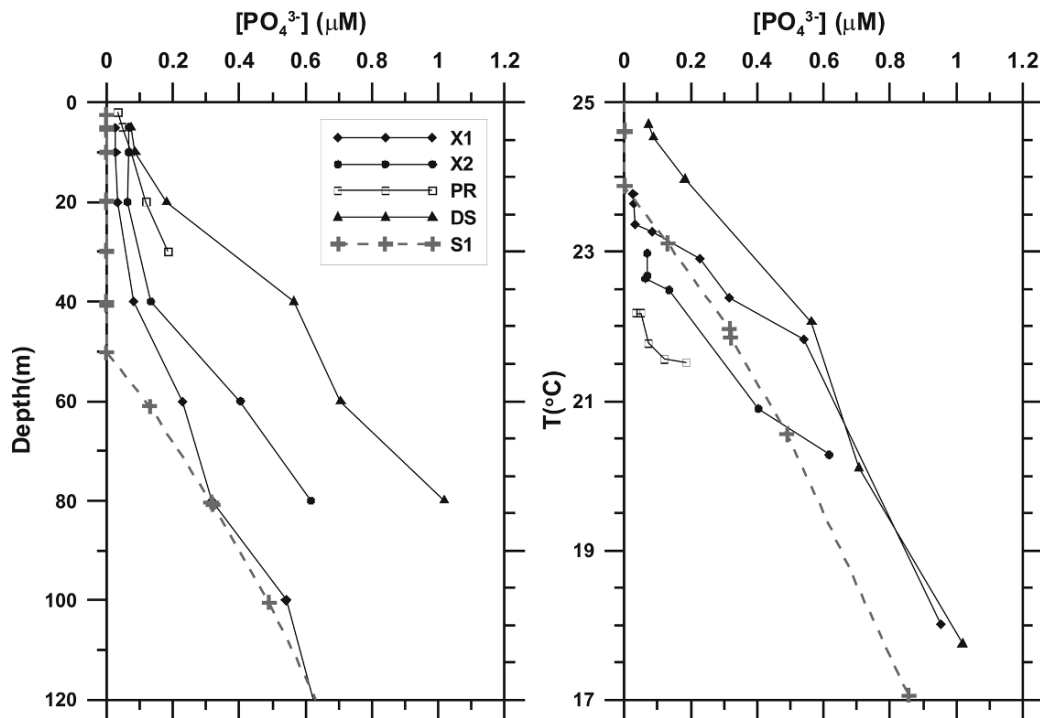


**Fig. 8.6.8** (a) Profiles of phosphate observed in the northern SCS in March 2000 and March 2002. The station localities are shown in Fig. 8.6.1. (b) Relationships between temperature and

phosphate at the same stations, indicating enrichment of phosphate in the upper water column at stations near the shelf break. The enrichment is attributed to internal wave breaking

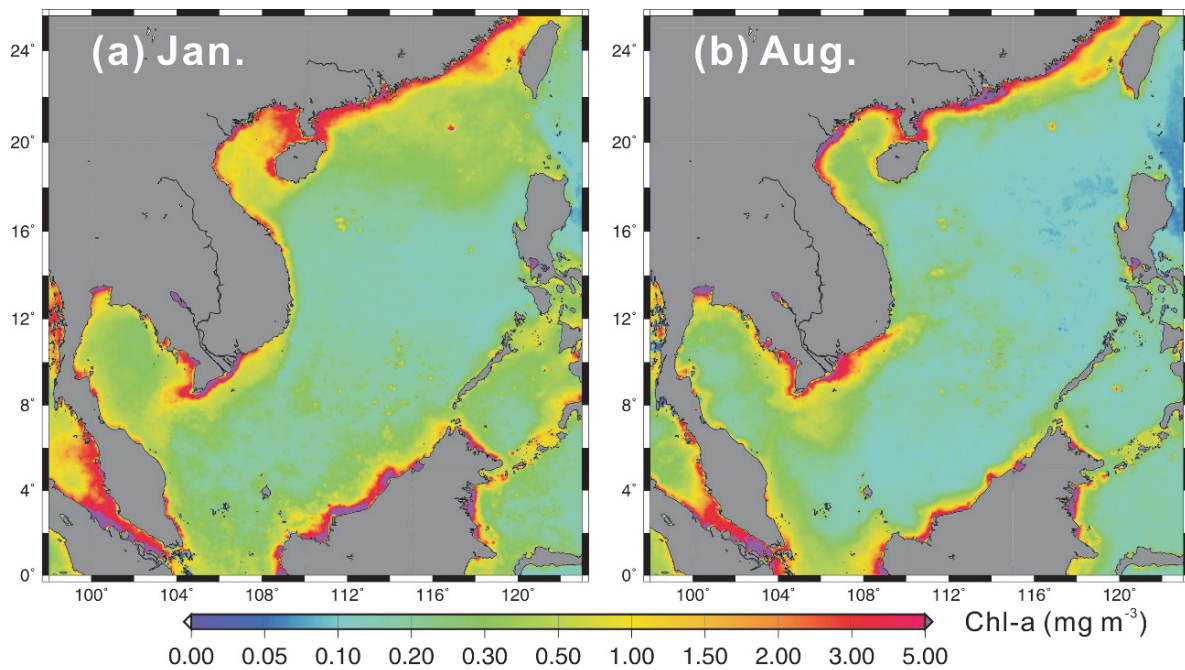


**Fig. 8.6.9** Composite Chl-a distribution derived from SeaWiFS ocean color imagery from 1998 to 2000 for (a) January and (b) August. In January the elevated Chl-a concentrations in the

northern SCS northwest of Luzon and in the southern SCS over the Sunda Shelf are attributed to monsoon-induced upwelling. In August a similar process occurred off Vietnam

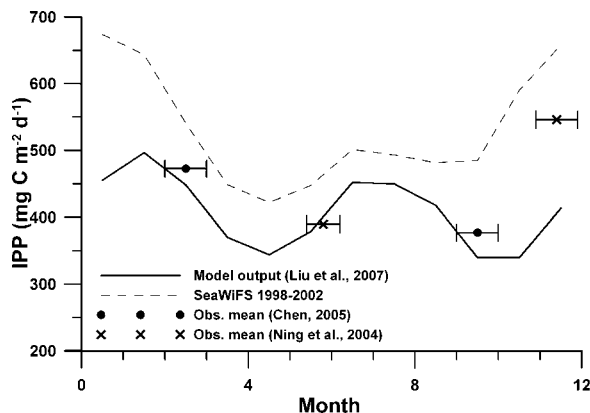


**Fig. 8.6.10** Monthly mean primary productions (in units of  $\text{mg C m}^{-2} \text{d}^{-1}$ ) in the SCS predicted by the biogeochemical model of the SCS. Also plotted are observed average values and values calculated from SeaWiFS data (Liu et al. 2007a)

during the monsoons and minima (down to monthly mean of  $422 \text{ mg C m}^{-2} \text{d}^{-1}$ ) during the inter-monsoons (Fig. 8.6.10). The estimated monthly mean IPP values compare favorably with observed mean values in different seasons over the entire SCS except that for winter. The observed mean value for December (Ning et al. 2004) was considerably higher than the model prediction. Because the observed values varied in a wide range ( $146\text{--}1,605 \text{ mg C m}^{-2} \text{d}^{-1}$ ), the mean value could be biased by a few very high values observed in the coastal zone. On the other hand, the monthly mean wind data used in the model do not properly represent the episodic strong winds under the winter monsoon (Liu et al. 2002) and may result in too weak a vertical mixing and, therefore, may cause underestimation of IPP. The annual mean is  $406 \text{ mg C m}^{-2} \text{d}^{-1}$  with an average of  $390 \text{ mg C m}^{-2} \text{d}^{-1}$  for the deep region ( $>200 \text{ m}$ ) and  $429 \text{ mg C m}^{-2} \text{d}^{-1}$  for the shallow region ( $<200 \text{ m}$ ).

Using sea surface Chl-*a* concentrations derived from SeaWiFS imagery, we calculated the primary production values for the SCS with the algorithm of Behrenfeld and Falkowski (1997). The average monthly IPP values are calculated from 5 years (1998–2002) of SeaWiFS data (Fig. 8.6.10). The results show similar seasonal trend as the model output, but the values are all higher than observed mean values as well as the model output. The overestimation is attributed to the overestimated Chl-*a* concentrations derived from SeaWiFS imagery in the coastal zone, probably due

to interference from colored organic matter and resuspended sediments (Sathyendranath 2000).

The export production may be considered in two categories: the SCS proper and the shelf. The export of biogenic particles in the former region relies on the vertical sinking process, while that in the latter region may be achieved by lateral transport across the shelf break. The modeled average flux of sinking particles at  $125 \text{ m}$  in the SCS proper is  $33 \text{ mg C m}^{-2} \text{d}^{-1}$  (Liu et al. 2002), which is about 10% of the modeled mean primary production. Chen et al., (2004d) conducted  $^{15}\text{NO}_3^-$  uptake experiments on cruises in the northern SCS in March 2000 and March 2001 and found values of the *f*-ratio, which is defined as new production/primary production, in the range of 0.14–0.60 with a mean of 0.36. The modeled POC export and, therefore, *f*-ratio, reaches a maximum in March, especially in the northern SCS, where upwelling is still active in March. The annual average *f*-ratio is probably considerably smaller. Chen (2004b) used POC inventories coupled with the scavenging rate of excess  $^{234}\text{Th}$  in the upper water column of the northern SCS (Lin 2003) to predict a mean POC flux of about  $96 \text{ mg C m}^{-2} \text{d}^{-1}$ , which gives an export ratio of about 0.27. For this study, the export ratio of the SCS proper is assumed to be 0.18, which is the median value of the range from 0.10 to 0.36 and close to that (0.19) predicted by the coupled ROMS–CoSINE model (Liu and Chai 2009). Then the export flux is  $69 \text{ mg C m}^{-2} \text{d}^{-1}$  ( $2.10 \text{ mol C m}^{-2} \text{yr}^{-1}$ ); the total export is  $4,182 \text{ Gmol C yr}^{-1}$ .

According to the improved SCS biogeochemical model (Liu et al. 2007a) the mean water column PP in the SCS shelf is estimated to be  $413 \text{ mg C m}^{-2} \text{d}^{-1}$  for the region with water depth less than  $100 \text{ m}$ , which has a total area of  $1.356 \times 10^{12} \text{ m}^2$ . The export of shelf production across the shelf is difficult to determine. Taking a conservative estimate, we assume the export ratio to be 0.1 giving total export at  $1,706 \text{ Gmol C yr}^{-1}$ .

A fraction of the shelf production is deposited and buried in the sediments. Kao et al. (2006) reported enhanced organic carbon burial that may account for 2.3% of total primary production on the continental shelf and slope in the SCS off southwestern Taiwan in rapidly accumulating sediments because of the rich supply of sediments from rivers. Since high sediment production is widespread in the surrounding landmasses of the SCS, similar processes may occur over the entire SCS shelf–slope region. For the shelf ( $0\text{--}100 \text{ m}$ ), upper slope ( $100\text{--}700 \text{ m}$ ), and deep basin

(>700 m), we assume sedimentation rates of 600, 100, and 50 g m<sup>-2</sup> yr<sup>-1</sup>, respectively, which are based on the observed relationship between sediment accumulation rate and depth (Kao et al. 2006). For the three areas we assume total organic carbon (TOC) contents of 0.4, 0.5, and 0.8%, respectively, which are based on the relationship between TOC and depth reported by Lai and Liu (1994). Then we can get a total organic carbon burial of 342 Gmol C yr<sup>-1</sup> or 4.1 Tg yr<sup>-1</sup>. If half of that is from marine origin as observed by Kao et al. (2006), it accounts for about 0.4% of the total PP.

### 8.6.3.2 Air–Sea CO<sub>2</sub> Exchange

Air–sea exchange of CO<sub>2</sub> in the SCS has been investigated by various projects. For the shallow region (depth <200 m), the distribution of pCO<sub>2</sub> in the surface waters of the northern SCS has been measured on repeated cruises from summer 2000 to fall 2002 (Zhai et al. 2005a,b). They were generally higher than atmospheric pCO<sub>2</sub> with ΔpCO<sub>2</sub> up to 100 μatm in the offshore region. Nearshore pCO<sub>2</sub> showed more variability mostly at levels considerably higher than the air pCO<sub>2</sub>. The estimated overall average CO<sub>2</sub> flux for the shelf region in the northern SCS was 1.2 mol C m<sup>-2</sup> yr<sup>-1</sup> (Zhai et al. 2005a,b). This value is assumed to represent all shallow regions in the SCS for the biogeochemical flux calculation.

Carbonate chemistry has been studied at the SEATS station on bimonthly to quarterly cruises since September 1999. More recently underway pCO<sub>2</sub> measurements have been conducted on the time series cruises. Results from 19 cruises between September 1999 and October 2003 showed the air–sea flux of CO<sub>2</sub> varying seasonally (Fig. 8.6.11). The general pattern shows the average sea–air flux of 1.1 ± 0.2 mol m<sup>-2</sup> yr<sup>-1</sup> in summer and average flux of -1.4 ± 0.4 mol m<sup>-2</sup> yr<sup>-1</sup> in winter. The seasonal changes in fCO<sub>2</sub> may be accounted for mostly by the seasonal changes in water temperature (~ 6°C). However, the associated air–sea exchange flux is also controlled by wind speed, which is much stronger in winter (Fig. 8.6.7a). Annually, the air–sea exchange of CO<sub>2</sub> at the SEATS station is nearly in balance, but the stronger winter monsoon makes the net transfer a very weak sink (around -0.02 mol C m<sup>-2</sup> yr<sup>-1</sup>). This value is assumed to rep-

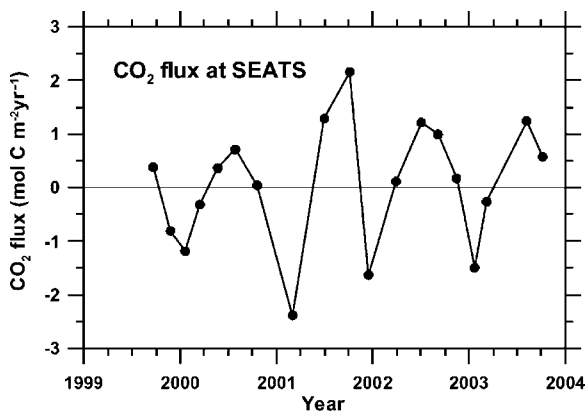


**Fig. 8.6.11** Fluxes of CO<sub>2</sub> (in units of mol C m<sup>-2</sup> yr<sup>-1</sup>) during air–sea exchange observed at the SEATS site (Tseng et al. 2007)

resent the SCS interior for the biogeochemical flux calculation.

### 8.6.3.3 Nitrogen Cycle

It has been observed that nitrogen fixation occurs in the SCS (Saino 1977; Voss et al. 2006) and the regenerated nitrate from nitrogen fixers is present in the thermocline water in the SCS (Wong et al. 2002), but the rate of nitrogen fixation is difficult to quantify due to the patchiness of nitrogen-fixing organisms, such as *Trichodesmium*. Liu et al. (1996) proposed using the nitrogen isotope balance to estimate the rate of nitrogen fixation. In short, the method is based on mass balance and isotope balance for nitrogen in the water column as follows:

$$F_f + F_{\text{DIN}} = F_{\text{PN}}$$

$$F_f \delta_f + F_{\text{DIN}} \delta_{\text{DIN}} = F_{\text{PN}} \delta_{\text{PN}}$$

where  $F$  represents the flux and  $\delta$  represents the mean  $\delta^{15}\text{N}$  value and the subscript  $f$  stands for nitrogen fixation, DIN stands for upwelled nitrate from the subsurface layer, and PN stands for sinking particulates. This model is valid for the SCS interior, where isotope effects due to lateral fluxes from river discharges and exchange with the open ocean are probably negligible.

The mean flux of sinking PN (mg N m<sup>-2</sup> d<sup>-1</sup>) is calculated from the mean primary production (390 mg C m<sup>-2</sup> d<sup>-1</sup>) using the relationship reported by

Pace et al. (1987):

$$F_{\text{PN}} = 0.432 Z^{-0.843} \text{PP}^{1.123}$$

where  $Z$  is the depth in meters and  $\text{PP}$  is primary production in  $\text{mg C m}^{-2} \text{d}^{-1}$ . The isotopic composition of the sinking  $\text{PN}$  is assumed to be 3.7‰, which is the average of the observed nitrogen isotopic composition of sinking particles collected with sediment traps in the northern SCS (Hu 2007). The isotopic composition of nitrate at 100 m depth at the SEATS station is 4.4‰ (Wong et al. 2002). The flux of fixed nitrogen is calculated to be  $0.78 \text{ mg N m}^{-2} \text{d}^{-1}$  or  $20 \text{ mmol N m}^{-2} \text{yr}^{-1}$ . This estimate is similar to those ( $31\text{--}51 \text{ mmol N m}^{-2} \text{yr}^{-1}$ ) reported for the Hawaii Ocean time-series station (Karl et al. 1997). If this estimate represents the average condition in the entire SCS, the total nitrogen fixation rate is  $67 \text{ Gmol N yr}^{-1}$ .

Alternatively the flux of nitrogen fixation may be estimated from the consumption of phosphate in the surface water of the SCS, where the N:P ratio of dissolved inorganic nutrients ranges from 0.2 to 3.5 with a mean of 1.2 (Chen et al. 2004d), indicating severe nitrogen depletion. It has been observed that the soluble reactive phosphate (SRP) in surface water at SEATS decreases with time from 24 to about 6 nM over the period March–July 2000 (Wu et al. 2003). A similar trend was observed again in 2002 (Su 2004). If the consumption of SRP is attributed to nitrogen fixation during the warm period over the annual cycle, we calculate the flux of nitrogen fixed in the top 20 m to be  $16 \text{ mmol N m}^{-2} \text{yr}^{-1}$  using a N:P ratio of 45 for the nitrogen fixers (Fennel et al. 2002). This is certainly the lower limit of the estimate, because the diffusive and aeolian fluxes of SRP are not considered. Nevertheless, this is consistent with the flux of nitrogen fixation based on the nitrogen isotope balance.

The flux of nitrogen removed during denitrification on the continental shelf has been estimated from the biogeochemical model of the SCS (Liu et al. 2007a). The average DIN flux removed during denitrification in the shelf region is  $71 \text{ mmol N m}^{-2} \text{yr}^{-1}$ . The value is similar to the denitrification rate of  $17\text{--}53 \text{ mmol N m}^{-2} \text{yr}^{-1}$  observed in the Baltic Sea (Stockenberg and Johnstone 1997). The total removal rate of DIN in the entire SCS is estimated to be  $96 \text{ Gmol N yr}^{-1}$ , of which 85% is attributed to the shallow region with water depth less than 200 m. The model also predicts the mean benthic nitrification rate

of  $1.06 \text{ mmol N m}^{-2} \text{d}^{-1}$ , which may support a productivity of  $84 \text{ mg C m}^{-2} \text{d}^{-1}$  of phytoplankton growth, about 21% of mean IPP.

## 8.6.4 Transports and Fluxes

Chen et al. (2001b) provide a synthesis of nutrient budgets for the SCS basin based on a box model. We follow the box model approach; instead of using one box, we divide the basin into three boxes, the surface zone (0–100 m), the intermediate layer (100–700 m), and the basin (>700 m) in order to explore different biogeochemical processes at different depth levels. In addition, we include new findings and information obtained from recent observational and modeling efforts for the synthesis. However, even with many new data available, the constraints on the rather large number of estimated fluxes and transports are hardly enough. The presented results represent the best description of a steady-state scenario that fits most, if not all, observed features.

### 8.6.4.1 Water and Salt Budget

The water exchanges between the SCS basin and the surrounding seas and between different levels in the SCS are depicted in Fig. 8.6.12. Based on information presented above, the water and salt budgets are constructed as shown in Table 8.6.2. Some remarks and discussion follow. The surface box represents the euphotic zone and the shelf; the intermediate layer encompasses the main thermocline and the upper slope; the deep box represents the lower slope and deep basin of the SCS. There is considerable exchange of water through the entire section of the Luzon Strait; the net exchange is an inflow of 1.68 Sv, which is distributed among all three layers with the maximum inflow (1.06 Sv) in the surface layer and minimum (0.17 Sv) in the intermediate layer.

The surface box receives a large freshwater input from rain and river runoff. The salt balance is achieved primarily through the removal of low salinity water via the three major shallow outlets and through voluminous water exchange at the Luzon Strait. The salinity values are mostly taken from observations. The salinity

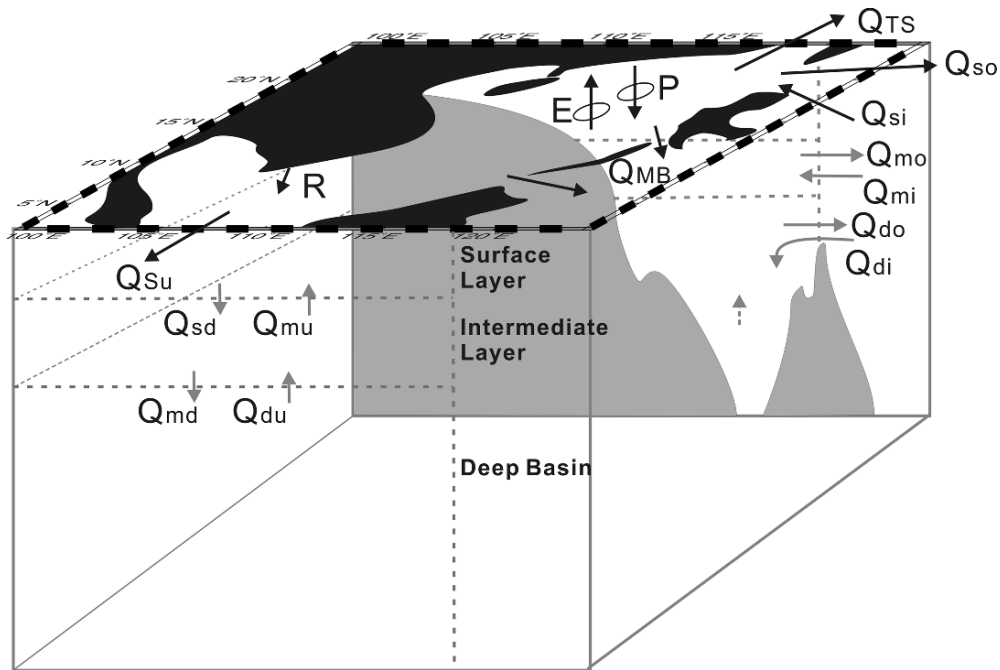


**Fig. 8.6.12** The box model of the SCS. The transports ( $Q$  terms) are explained in Table 8.6.2. The surface layer is the top

100 m; the intermediate layer is from 100 to 700 m; the basin is deeper than 700 m

of the outflow through the Taiwan Strait (34.0 psu) is the annual average (Chen 2001). The rather high salinity of the outflow through the Mindoro–Balabac Stratis (34.4 psu) represents both the surface water and the intermediate water (down to as deep as 420 m). The strong salinity gradient at the Luzon Strait makes the choice difficult. The salinity and the transport of surface inflow are taken from the model output described before, while those of the surface outflow are determined by balancing the water and salinity budget:

$$\begin{aligned} \Sigma Q_i = P + E + R + Q_{si} + Q_{so} + Q_{mu} + Q_{sd} + Q_{ST} \\ + Q_{Su} + Q_{MB} = 0 \text{ and } \Sigma Q_i \rho_i S_i = 0 \end{aligned}$$

where the terms of the transports ( $Q$ ) are explained in Table 8.6.2, and their values are positive for inflows and negative for outflows, and  $\rho_i$  and  $S_i$  represent density and salinity, respectively. The surface outflow calculated from the budget equations is 6.0 Sv, which is quite close to the model prediction of 5.78 Sv in the top 115 m. The estimated salinity of the outflow is relatively high (34.51 psu), in comparison with the surface water of the SCS interior (Fig. 8.6.4), suggesting that the outflow water has experienced mixing with

the intruding Kuroshio water before exiting the SCS proper through the Luzon Strait.

The volume transports of vertical water exchange between the surface layer and the immediate layer are as important as the lateral exchange transports. Estimation of these transports is partially based on 3-D modeling and partially based on salt and nutrient balances. The vertical water exchange has some significance in the salt budget, while its role in the nutrient budget is more important, because the nutrient gradient is stronger than the salinity gradient between the surface and the intermediate layer (Fig. 8.6.6). Details of the nutrient balance are described in the next subsection.

The intermediate layer exchanges waters with the overlying surface layer and the deep basin as well as the intermediate layer of the WPS. This lateral exchange through the Luzon Strait has the largest transports. The vertical transports are determined either by 3-D modeling or by the nutrient budgeting to be explained later, while the lateral outflow is taken from the model output and inflow is determined by water and salt balance. The inflow (9.62 Sv) is similar to the modeled inflow of 9.9 Sv. The net transport of lateral exchange is a small inflow of 0.17 Sv.

**Table 8.6.2** Volume transports and budgets of water, salt, nitrogen, and phosphorus in the SCS

Processes	Water (Sv)	Density (kg m <sup>-3</sup> )	S (psu)	Salt (Gt yr <sup>-1</sup> )	[DIN] (μM)	N (Gmol yr <sup>-1</sup> )	[DIP] (μM)	P (Gmol yr <sup>-1</sup> )
Surface layer (0–100 m)								
Precipitation (P)	0.20	1			3.6	23	0.16	1.0
Evaporation (E)	-0.13	1						
Runoff (R)	0.04	1	0.22	0.29	49.7	64	0.99	0.8
N fix						67		
Typhoon mixing				23	22.2	40	1.58	3.0
Internal wave breaking				13	35.0	23	2.58	1.7
Surface-in ( $Q_{si}$ )	7.05	1.022	34.70	7890	0.6	133	0.13	27.8
Surface-out ( $Q_{so}$ )	-6.00	1.023	34.51	-6685	1.3	-246	0.17	-31.4
Surface-down ( $Q_{sd}$ )	-4.48	1.027	34.55	-5016	6.4	-908	0.47	-66.7
Mid-up ( $Q_{mu}$ )	5.00	1.027	34.60	5607	12.0	1893	0.80	126.9
Taiwan Strait ( $Q_{TS}$ )	-1.10	1.022	34.00	-1206	1.1	-39	0.16	-5.4
Sunda Shelf ( $Q_{Su}$ )	-0.38	1.021	33.00	-404	1.0	-12	0.15	-1.8
Mindoro–Balabac ( $Q_{M-B}$ )	-0.20	1.022	34.40	-222	2.0	-13	0.21	-1.3
Burial						-41		-2.6
Denitrification						-96		
Particle flux at 100 m						-644		-40.2
Shelf export						-270		-16.9
Intermediate layer (100–700 m)								
Particle flux at 100 m						644		40.2
Shelf export						270		16.9
Surface-down ( $Q_{sd}$ )	4.48	1.027	34.55	5016	6.4	908	0.47	66.7
Mid-up ( $Q_{mu}$ )	-5.00	1.027	34.60	-5607	12.0	-1893	0.80	-126.9
Mid-in ( $Q_{mi}$ )	9.62	1.027	34.60	10788	21.6	6567	1.52	461.8
Mid-out ( $Q_{mo}$ )	-9.45	1.027	34.60	-10597	22.2	-6620	1.58	-471.7
Mid-down ( $Q_{md}$ )	-2.40	1.027	34.60	-2691	27.3	-786	1.98	-57.0
Deep-up ( $Q_{du}$ )	2.75	1.028	34.60	3087	34.0	1121	2.50	82.6
Burial						-3		-0.2
Denitrification						-10		
Particle flux at 700 m						-173		-10.8
Deep basin (>700m)								
Particle flux at 700 m						173		10.8
Mid-down ( $Q_{md}$ )	2.40	1.027	34.60	2691	27.3	786	1.98	57.0
Deep-up ( $Q_{du}$ )	-2.75	1.028	34.60	-3087	34.0	-1121	2.50	-82.6
Deep-out ( $Q_{do}$ )	-0.50	1.028	34.60	-561	35.0	-210	2.58	-15.5
Deep-in ( $Q_{di}$ )	0.85	1.028	34.60	954	38.0	387	2.77	28.2
Burial						-7		-0.5
Denitrification						-7		

The water exchange in the basin is constrained by the deep inflow of 0.85 Sv, which accounts for the presumed residence time of 50 years for the deep basin water below the sill depth. This inflow is balanced by a lateral outflow around 1,000 m as suggested by Chao et al. (1996a) and a net upwelling transport, which is determined from the nutrient balance.

The turnover of water in the SCS is relatively quick. If only the exchange with the outside is considered,

the total inflow or outflow for the surface layer is about 7.3 Sv (Table 8.6.2), which gives a turnover time of about 1.1 years for a volume of  $0.26 \times 10^{15} \text{ m}^3$ . Alternatively, the effective inflow may be determined from the mean salinity of the inflow (34.6 psu) and the total freshwater input of 0.11 Sv; the mixture of the two end members should give the mean salinity of the surface layer (33.8 psu). The calculated effective inflow is 4.8 Sv, which gives a turnover time of 1.8

years. The actual residence time is probably between the two estimates. For the intermediate layer, the total inflow or outflow is about 9.6 Sv (Table 8.6.2), which gives a turnover time of 3.8 years for a volume of  $0.98 \times 10^{15} \text{ m}^3$ . This is consistent with the estimate of a residence time of less than a decade from the chlorofluorocarbon study in the SCS (Lee, B.-S. unpublished data).

#### 8.6.4.2 Biogeochemical Fluxes

The biogeochemical fluxes presented in Table 8.6.2 include those of dissolved inorganic nitrogen and phosphorus associated with volume transports as well as the fluxes of nitrogen and phosphorus across the air–sea interface, the surface–intermediate water interface, and the water–sediment interface. Additional estimates of carbon, nitrogen, phosphorus, and sediment fluxes are presented in Table 8.6.3.

In the surface layer, the major inflow of nutrients is from the vertical exchange with the intermediate water, which contributes both salt and nutrients to the surface layer. The net upwelled water not only balances the salt budget but also compensates for the loss of N and P via the sinking particle fluxes, i.e., the biological pump, and the shelf export, i.e., the shelf pump. The efficiency of the biological pump ( $f = 0.18$ ) is estimated from measurements of new production, particle fluxes derived from  $^{234}\text{Th}$  deficiency, and biogeochemical modeling. The strength of the shelf pump is assumed to be 10% of the total shelf PP. The net transport of the vertical exchange is determined by balancing the budgets for both N and salt, simultaneously. The transports for phosphorus are determined from those of nitrogen. For the sinking particles, a N:P ratio of 16 is assumed (Redfield et al. 1963). For the dissolved inorganic nutrients, the N:P ratio is determined from observations at the SEATS station (Fig. 8.6.13). To our surprise the budget so constructed for phosphorus is balanced and lends strong support to the nutrient budget presented here. It is noted that the total inflows of DIN ( $1,315 \text{ Gmol yr}^{-1}$ ) and DIP ( $70 \text{ Gmol yr}^{-1}$ ) are considerably larger than the fluxes of PON and POP exported to the intermediate layer, suggesting incomplete utilization of the nutrient input.

In addition to vertical water exchange, there are other nutrient pumping mechanisms, namely, strong wind-driven mixing during typhoons and internal wave

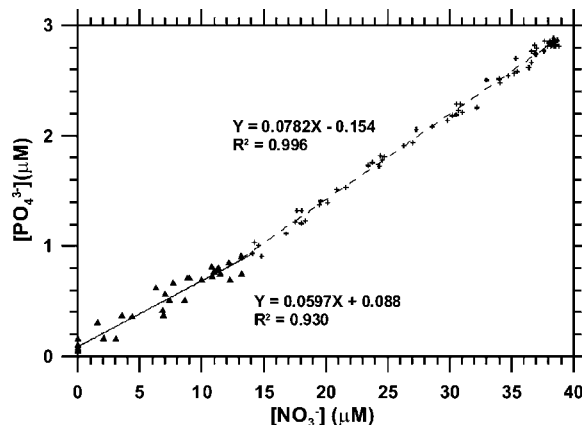


**Fig. 8.6.13** The nitrate–phosphate relationship observed at the SEATS station in different seasons (Su 2004). The phosphate concentration was analyzed with the MAGIC procedure (Karl and Tien 1992). The data points are separated into two groups for linear regression analysis in order to obtain tighter relationships

breaking. At present, we are unable to estimate the contribution from mesoscale eddies to nutrient pumping. We have taken into consideration these extra transports in the nutrient budget. For alternative nutrient pumps, though they are limited in capacity and spatial coverage, their combined strengths are not negligible. Besides nutrient pumping, these processes may also bring salt to the surface layer. The salt transports are calculated in proportion to the DIN transports with the same salt to DIN relationship as the vertical water exchanges.

Aside from internal nutrient source, there are allochthonous nutrient sources, including riverine fluxes, dry and wet deposits, and nitrogen fixation. The combined allochthonous sources of nitrogen ( $154 \text{ Gmol N yr}^{-1}$ ) are equivalent to about 18% of the internal supply. By contrast, the allochthonous input of DIP is quite limited ( $1.8 \text{ Gmol yr}^{-1}$ ). However, other forms of allochthonous phosphorus, such as particulate phosphorus discharged from rivers, could be important to make up for the phosphorus deficiency (Liu et al. 2008) and deserve further investigation.

As pointed out by Chen et al. (2001b), the outflow from the SCS serves as a nutrient source to the oligotrophic WPS due to the elevated level of nutrients in the surface and intermediate water in the SCS. The net outflow of DIN through the Luzon Strait to the Kuroshio water reaches  $113 \text{ Gmol N yr}^{-1}$ , which corresponds to a capacity of carbon fixation of  $750 \text{ Gmol C yr}^{-1}$  or  $9.0 \text{ Tg C yr}^{-1}$ . Besides the outflow

**Table 8.6.3** Biogeochemical fluxes in the SCS

Process	Area (10 <sup>12</sup> m <sup>2</sup> )	C-flux (mol m <sup>-2</sup> yr <sup>-1</sup> )	C (Gmol yr <sup>-1</sup> )	N-flux (mmol m <sup>-2</sup> yr <sup>-1</sup> )	N (Gmol yr <sup>-1</sup> )	P-flux (mmol m <sup>-2</sup> yr <sup>-1</sup> )	P (Gmol yr <sup>-1</sup> )	Sediment acc. rate (g m <sup>-2</sup> yr <sup>-1</sup> )	Sediments (Mt yr <sup>-1</sup> )	CaCO <sub>3</sub> (Mt yr <sup>-1</sup> )
Surface layer (0–100 m)										
Air–sea	3.35	0.57(outgasing)	1,893							
PP(interior)	2.00	11.88	23,699	1,793	3,577	112	224			
PP(shelf)	1.36	13.21	17,916	1,994	2,704	125	169			
N fix	3.35			20	67					
Dry-wet deposits	3.35			7	23	0.3	1.1			
Burial	1.36	0.20	271	30	41	1.9	3	600	814	81
Denitrification	1.36			71	96					
Particle flux at 100 m	2.00	2.14	4,266	323	644	48.7	97			
Shelf export	1.36	1.32	1,792	199	270	30.1	41			
Intermediate layer (100–700 m)										
Burial	0.51	0.04	21	6	3	0.4	0.2	100	51	15
Denitrification	0.51			20	10					
Particle flux at 700 m	1.49	0.76	1,126	114	170	17.2	25.7			
Deep basin (>700m)										
Burial	1.49	0.03	50	5	7	0.3	0.5	50	75	15
Denitrification	1.49			5	7					

through the Luzon Strait, outflows through other channels also carry sizable amounts of nutrients. The outflow through the Taiwan Strait carries  $39 \text{ Gmol yr}^{-1}$  of DIN, which matches the annual mean transport estimated from two contrasting seasons by Chen et al. (2001b). The N:P ratio of 7.1 falls between the estimates of 5.4–7.6 for the SCS outflow through the Taiwan Strait (Liu et al. 2000c; Chung et al. 2001).

For the intermediate layer, the lateral exchange results in little net nutrient transport, while the vertical fluxes are much more important. The export fluxes from the surface layer are very important. We assume that the export fluxes of PON and POP from the shelf are deposited on the slope, where they are either regenerated or buried. Some of the regenerated PON is removed during denitrification. The fluxes from the central portion of the SCS may sink to the deep basin ( $>700 \text{ m}$ ). However, any particles deposited on the slope have the same fate as the shelf exports. The flux of organic carbon that may survive decomposition in the water column is calculated according to the POC–ballast relationship proposed by Armstrong et al. (2002):

$$(Z) = F_{\text{inf}} + [F(Z_0) - F_{\text{inf}}] \exp(-(Z - Z_0)/d)$$

where  $F(Z)$  is the flux at depth ( $Z$ ),  $Z_0$  is the bottom of the euphotic zone,  $F_{\text{inf}}$  is the flux of organic carbon protected by the ballast minerals that may reach great depth, and  $d$  is the scaling length of organic carbon decomposition (480 m).  $F_{\text{inf}}$  may be estimated from the ballast flux ( $F_B$ ):

$$F_{\text{inf}} = \rho F_B$$

where  $F_B$  is assumed to be the same as the sediment accumulation rate for the deep basin ( $50 \text{ g m}^{-2} \text{ yr}^{-1}$ ) and  $\rho$  is a constant (0.052). The calculated POC flux at 700 m ( $0.69 \text{ mmol C m}^{-2} \text{ yr}^{-1}$ ) is 37% of the flux at 100 m. The sinking fluxes of PON and POP at 700 m are calculated from the POC with the Redfield ratio.

Based on the same assumptions for organic carbon burial, the fluxes of sediment accumulation are calculated and summarized in Table 8.6.3. The burial fluxes of nitrogen and phosphorus are calculated using an average C:N:P ratio of 106:16:1 (Redfield et al. 1963). The burial of carbonate is calculated with the assump-

tion of  $\text{CaCO}_3$  contents of 10, 30, and 25% for the shelf, upper slope, and deep basin, respectively (Su 1989). Despite the rather crude calculation, the sum of the total riverine loading of sediments ( $854 \text{ Mt yr}^{-1}$ ) and the total burial of  $\text{CaCO}_3$  ( $111 \text{ Mt yr}^{-1}$ ) matches the total sediment accumulation rate of  $939 \text{ Mt yr}^{-1}$  reasonably well.

For N and P, we have provided a rather complete account of their budgets with the exceptions of dissolved organic species, but for carbon we have provided only a partial budget that did not take into account the dissolved species, including DIC and DOC due to insufficient data. Nevertheless, the partial budget of carbon still provides us with new insight into the carbon cycle.

The current assessment reveals the SCS to be a net source of  $\text{CO}_2$ ; however, the lack of sufficient observations during high wind conditions in winter, when the SCS interior has been observed as a  $\text{CO}_2$  sink, makes accurate assessment of net  $\text{CO}_2$  transfer difficult. It is noted that the total export production ( $6,057 \text{ Gmol yr}^{-1}$ ) exceeds the riverine input of organic carbon ( $633 \text{ Gmol yr}^{-1}$ ) by an order of magnitude (Table 8.6.3). If half of the buried organic carbon is from terrigenous origin as that observed off southwestern Taiwan (Kao et al. 2006), about 60% of terrigenous POC is decomposed in the ocean. Nitrogen fixation accounts for about 1% of nitrogen needed for primary production and 7% for export production.

The remineralization rate of particulate organic matter (POM) below the euphotic zone may be calculated from the sinking fluxes of particulate organic carbon, if all sinking organic particles that do not sink to deeper waters or get buried in sediments are remineralized within the SCS. The net input of particulate organic carbon to the intermediate layer is  $4,810 \text{ Gmol yr}^{-1}$  and that to the deep basin is  $979 \text{ Gmol yr}^{-1}$ . Remineralization rates of 4.9 and  $0.34 \text{ mmol C m}^{-3} \text{ yr}^{-1}$ , respectively, are attained in the intermediate layer (100–700 m) and the deep layer ( $>700 \text{ m}$ ). They correspond to oxygen consumption rates of 6.4 and  $0.44 \text{ meq m}^{-3} \text{ yr}^{-1}$ , respectively. The latter rate is in reasonable agreement with that ( $0.59 \pm 0.12 \text{ meq m}^{-3} \text{ yr}^{-1}$ ) estimated for the water at 2,000 m by Chen et al. (2001b). A fraction of organic carbon consumed is attributed to denitrification and other benthic processes.

### 8.6.5 Summary

Although the SCS is a semi-enclosed water body, the water exchange with the surrounding seas is rapid. The surface layer (0–100 m) has a water residence time of 1–2 years, the intermediate layer (100–700 m) has residence time of 3–10 years, and the basin water (>2,000 m) has a residence time of about 50 years. The alternating monsoons drive upwelling and downwelling in different parts of the basin resulting in extensive vertical mixing in the upper 1,000 m, while net upwelling results in an upward transport of nutrients. The upwelling is matched with a deep inflow of 0.85 Sv from the WPS. The lateral exchange of water in the surface layer results in net export of DIN ( $177 \text{ Gmol yr}^{-1}$ ) and DIP ( $12 \text{ Gmol yr}^{-1}$ ); these exports are supported by nutrient inflow in the intermediate and deep layers.

The mean primary production is estimated to be  $13.2 \text{ mol C m}^{-2} \text{ yr}^{-1}$  for the shelf (<100 m) and  $11.9 \text{ mol C m}^{-2} \text{ yr}^{-1}$  for the interior (>100 m). The total PP is  $42 \text{ Tmol C yr}^{-1}$  and the estimated export fraction is 0.14; these estimates need verification, especially shelf exports. The remineralization rate of the exported particulate organic matter is estimated to be  $4.9 \text{ mmol C m}^{-3} \text{ yr}^{-1}$  for the intermediate layer (100–700 m) and  $0.34 \text{ mmol C m}^{-3} \text{ yr}^{-1}$  for the deep basin below 700 m. The burial of marine organic carbon accounts for about 0.4% of total PP, but enhanced burial efficiency in rapidly accumulating sediments could bring the percentage up to 2.3% (Kao et al. 2006). This process warrants further investigation because of the high sediment production in this region. The benthic remineralization may provide about 1/5 of the nutrient demand needed for primary production. The  $\text{CO}_2$  flux during air–sea exchange changes sign from positive (source) in summer to negative (sink) in winter. The estimated net transfer is a weak source ( $0.57 \text{ mol C m}^{-2} \text{ yr}^{-1}$ ). Because of the high variability of the flux and limited spatial coverage, a more extensive study of the  $\text{CO}_2$  fluxes is much needed.

The nitrogen cycle in the SCS is dynamic. The flux of nitrogen fixation ( $20 \text{ mmol N m}^{-2} \text{ yr}^{-1}$ ) accounts for 7.5% of the nitrogen needed for total export production. The total supply of allochthonous nitrogen ( $154 \text{ Gmol yr}^{-1}$ ), from  $\text{N}_2$  fixation, dry-wet deposits, and river runoff, is equivalent to 18% of the total

internal supply of nitrate to the surface layer. The allochthonous input of phosphorus in the dissolved form is limited, but terrigenous particulate phosphorus (Beusen et al. 2005) could be important to make up for the phosphorus deficiency and deserve further investigation. Because nitrogen supply from river loads occurs at the surface, but removal occurs on the seafloor, the effects of these biogeochemical processes on the carbon cycle are important topics for future study. The biggest missing pieces in this budgetary study are dissolved organic matter and dissolved inorganic carbon, which are among the foci of ongoing projects such as The South-East Asia Time-series Study (Wong et al. 2007) and The South China Sea Regional Carbon Pilot Project (Chen 2002a). Better understanding of the biogeochemistry is expected in the near future.

### 8.7 Tropical Coastal Seas of Australia and Papua New Guinea

Gregg J. Brunskill, I. Zagorskis  
and J. Pfitzner

We are developing mass balance models for C, N and P for the NW shelf and NE shelf of Australia and the Gulf of Papua in Papua New Guinea. These regions are examples of (1) an arid coastal plain with little human development and runoff, an ocean-dominated shelf; (2) small river inputs from agricultural river catchments to the Great Barrier Reef (GBR) lagoon; and (3) very large river inputs from wet tropical, tectonically active catchments to the Gulf of Papua. Where possible, we assemble components of the budget by measuring river input, productivity and respiration on the shelf, burial in shelf sediments and flux to sediment traps at the base of the continental shelf (=export). We infer fluxes from and to the atmosphere from mass balance equations.

---

G.J. Brunskill (✉)  
84 Alligator Creek Road, Alligator Creek, Queensland 4816,  
Australia  
e-mail: g.brunskill@aims.gov.au